

Article

The Effects of the Long-Term Freeze–Thaw Cycles on the Forms of Heavy Metals in Solidified/Stabilized Lead–Zinc–Cadmium Composite Heavy Metals Contaminated Soil

Zhongping Yang ^{1,2,3,*} , Jiazhao Chang ^{1,2,3}, Xuyong Li ^{1,2,3}, Keshan Zhang ^{1,2,3} and Yao Wang ^{1,4}

¹ School of Civil Engineering, Chongqing University, Chongqing 400045, China; changjiazhao@cqu.edu.cn (J.C.); lixuyong@cqu.edu.cn (X.L.); zhangkeshan1999@163.com (K.Z.); a_yao0218@163.com (Y.W.)

² Key Laboratory of New Technology for Construction of Cities in Mountain Area, Chongqing University, Ministry of Education, Chongqing 400045, China

³ National Joint Engineering Research Center for Prevention and Control of Environmental Geological Hazards in the TGR Area, Chongqing University, Chongqing 400045, China

⁴ China Machinery China Union Engineering Co., Ltd., Chongqing 400045, China

* Correspondence: yang-zhp@163.com; Tel./Fax: +86-(023)-65120728

Abstract: Heavy metals (HMs) exist in nature in different forms, and the more unstable the form of an HM, the higher its toxicity and bioavailability. The content of HMs in stable fractions can increase significantly through the stabilization/solidification (S/S) technology. Still, external environments such as freeze–thaw (F–T) cycles will affect the stability of HMs directly. Therefore, a long-term F–T study of S/S Pb–Zn–Cd composite HM-contaminated soil was conducted under six conditions (0, 3, 7, 14, 30, and 90 cycles) with each F–T cycle process up to 24 h. The improved Tessier method was employed, and the results show that the S/S technology makes HMs transform to a more stable fraction. Still, the transformation efficiency is different for each HM. More than 98% of lead and zinc were converted to stable forms, while for cadmium, there are only 75.1%. Meanwhile, the S/S HMs were rapidly transformed into unstable forms at 0–14 cycles, but after 14 cycles, the transformation speed was significantly reduced. Among stable forms, it is mainly that the carbonate-bound fraction of HMs changes to unstable forms, and the characteristic peaks of carbonate stretching vibration were found at 874 cm^{−1}, and 1420 cm^{−1} by Fourier infrared spectroscopy proves the presence of carbonate-bound substances. As a result of this study, the change trend of contaminated soil with S/S HMs under the effect of long-term F–T cycle was revealed, and the crisis point of pollution prevention and control was found, which provides some theoretical basis for the safety of soil remediation project.

Keywords: long-term freeze–thaw cycles; composite heavy metal contamination; morphological analysis; solidification/stabilization



Citation: Yang, Z.; Chang, J.; Li, X.; Zhang, K.; Wang, Y. The Effects of the Long-Term Freeze–Thaw Cycles on the Forms of Heavy Metals in Solidified/Stabilized Lead–Zinc–Cadmium Composite Heavy Metals Contaminated Soil. *Appl. Sci.* **2022**, *12*, 2934. <https://doi.org/10.3390/app12062934>

Academic Editors: Bing Bai and Dibyendu Sarkar

Received: 6 February 2022

Accepted: 10 March 2022

Published: 13 March 2022

Publisher's Note: MDPI stays neutral with regard to jurisdictional claims in published maps and institutional affiliations.



Copyright: © 2022 by the authors. Licensee MDPI, Basel, Switzerland. This article is an open access article distributed under the terms and conditions of the Creative Commons Attribution (CC BY) license (<https://creativecommons.org/licenses/by/4.0/>).

1. Introduction

Because of considerable migration depth, complex migration mechanism, sizeable spatial variability, strong concealment, and resistance to degradation of heavy metals (HMs), its high-concentration and high-risk pollutants in the soil are extremely difficult to repair and manage and are called “chemical time bombs” [1–3]. In recent years, the remediation of soil HM pollution has been an environmental topic worthy of attention. Studies have shown that HM pollutants may cause changes in soil structure, such as colloidal corrosion between soil particles, decrease in cementation strength, increase in clay content, resulting in increased soil compression, reduced liquid, and plastic limits, reduced shear strength (the reduction can reach about 35%), increased permeability, and the decreased bearing capacity [4–6]. In addition, the non-degradability of HMs leads to their accumulation in plants, animals, and humans along the biological chain [7–11].

Both pose a threat to human safety and health; therefore, it is imperative to control soil HM pollution [12]. There are two kinds of solutions to manage HM pollution in the soil. The first one is to directly reduce the concentration of HMs in the soil, and the second one is to reduce the possibility of HM migration. That means fixing them in place and reducing their biotoxicity by special treatments [13,14]. In this context, a series of treatment methods for HM-contaminated soils have emerged, such as S/S technology, displacement technology, soil leaching, incineration, solvent extraction, glass curing, and physical separation, emerged. Among them, solidification/stabilization (S/S) technology is the most widely used because of its cost-effective and simple operation [14,15].

The S/S technology of soil usually provides the ability to handle HMs through two aspects. On the one hand, the S/S technology has a direct effect on HMs. Chemical precipitation, physical encapsulation, adsorption, and other means occur between HMs and hydrations products of binders; on the other hand, the S/S technology directly affects soil, and indirectly affects HMs by changing the soil structure. The reduced permeability leads to reduced migration of HMs, then the stability of HMs in the soil can be achieved [15,16]. However, while enjoying the restorative power of S/S technology, one must also consider its environmental impact.

Considering this problem, three inorganic binders, cement, lime, and fly ash, were used in the current study to improve S/S efficiency while reducing carbon emissions and easing the burden of industrial waste disposal [17–19]. However, it should be noted that the use of binders should involve reasonable control of the amount: too little S/S has poor effect, but if the amount is too much it will not only increase the cost, but also change the physical and chemical properties of the soil, and even cause secondary pollution.

Starting from the mechanism of the S/S technology, it can be realized that this technology cannot reduce the concentration of HMs in the soil, but restricts the migration of pollution, or limits the effectiveness of pollutants. Based on this, it is necessary to track the follow-up progress of HMs after the use of S/S technology. In the internal system of S/S HM-contaminated soil, the type of soil [20], the type and content of HMs [21], the type and content of binders [22,23], the curing conditions [23], and the moisture content [24] all have an impact on the long-term stability of HMs. In various complex environments, such as carbonation [25], acid rain leaching [25–27], high salt groundwater infiltration [28,29], wetting and drying cycles [30–32], and F–T cycles [33–36], the stable forms of the contaminants in the S/S-contaminated soil is very likely to change or even fail, which causes the activation of HM pollutants in the soil, causing secondary pollution and affecting its engineering mechanical properties. Therefore, the environmental durability of S/S-contaminated soil is extremely sensitive to environmental changes. The impact of F–T cycles on S/S HM-contaminated soil will continue to be focused on in-depth in this study.

Freeze–thaw cycles mainly occur in seasonal frozen regions. The moisture in the soil constantly transforms between liquid and solid with the periodic change of temperature: through changes in the volume of water in different fractions, as well as the free migration of water, the pore structure and density of the soil are changed, which is one of the direct factors affecting the migration effect of HMs. In China, the area of seasonal permafrost is about 5.14 million square kilometers, accounting for 53 percent of the total land area [37]. According to the second national soil erosion remote sensing survey, China's F–T erosion area has reached 13.4% of the country's total area [38]. Because of the vast F–T area, it is of great practical significance to explore the influence of the F–T cycle on the S/S of HM-contaminated soil. After 12 F–T cycles, the leaching concentrations of Pb/Zn-contaminated soil and composite Zn–Pb-contaminated soil increased greatly [34]. The elastic modulus of silty clay and modified clay can be significantly reduced after four F–T cycles [39]. After conducting seven F–T cycles on silty clay, Wang et al. concluded that the number of F–T cycles had a great influence on the mechanical properties of soil [40]. Studies have confirmed that under the long-term effect of simple F–T cycles (180 cycles, 180 days), the unconfined compressive strength loss rate of cemented contaminated soil can reach more than 30%, and the concentration of HM ions in HM leaching solution can increase by more than 20% [18,41,42].

This research has been improved on this basis, and “long-term” is the keyword of this. Studying the condition of HMs in the soil during the long F–T cycle period, observing the S/S effect of the HMs is a good way to ensure the long-term use of the S/S soil. Effective control of HMs in soil under adverse conditions is of great significance to prevent secondary pollution of HMs. A maximum of 90 F–T cycles (90 days) was set up under the same F–T mode to explore the stability of HMs under long-term F–T cycles in this research.

After making up for the problem of short-term F–T, the situation of HMs in the soil has also been improved, and the transformation from single HM pollution to compound HM pollution research has been realized. According to a large number of studies, one source of pollution often produces multiple types of HM pollution [41–43]. As, Cd, Cr, Cu, Mn, Ni, Pb, Zn, and other HMs exist in the farmland soil of the Qixia mining area in Nanjing, China [44]. There are many HMs in the weathered coal gangue, and the surrounding land is also harmed by HMs such as Zn, Cd, and Cr. Research on a single HM-contaminated soil can no longer meet the actual needs. Therefore, in this study, three pollutants, Pb, Zn, and Cd, were added to the soil at the same time.

The adsorption–desorption, precipitation reaction, complexation reaction, and oxidation–reduction reaction between HMs and soil allow HMs to exist in different forms in soil, and different forms of HMs exhibit different toxicity and environmental behavior [45]. When HMs are in a less bioavailable form or a more stable form, their risk in the environment is low. Therefore, the content of each form of HMs can be used as an observation indicator to assess the risk of HMs in soil. The improved Tessier method was used to extract seven fractions of HMs in the soil in this study.

Based on the above analysis, the improved Tessier method was adopted to detect the content of various forms of HMs (Pb, Zn, and Cd) in the soil that had undergone six F–T cycle conditions (0, 3, 7, 14, 30, and 90 cycles) up to 90 days, and the functional groups were analyzed by Fourier transform infrared spectroscopy analysis tests. Meanwhile, the study assumes that the HMs are uniformly distributed in the soil, by controlling the particles of the original soil less than 1 mm, the mixing time of the preparation of contaminated soil longer than 5 min, and the error of X-ray fluorescence analyses (XRF) of the same batch of three concentrations less than 3%.

In this study, the safety of the S/S technology is investigated by using a near-actual high concentration of complex hinged HM-contaminated soil, the morphological changes of HMs as a variable of interest, and the F–T cycle effects that may occur in most of the global land as the influencing factor. The conclusions and laws drawn from this study provide more rigorous theoretical support for predicting the safety of seasonally S/S HM-contaminated soil use and provide favorable conditions for post-remediation reuse of contaminated soil [18].

2. Materials and Methods

2.1. Material

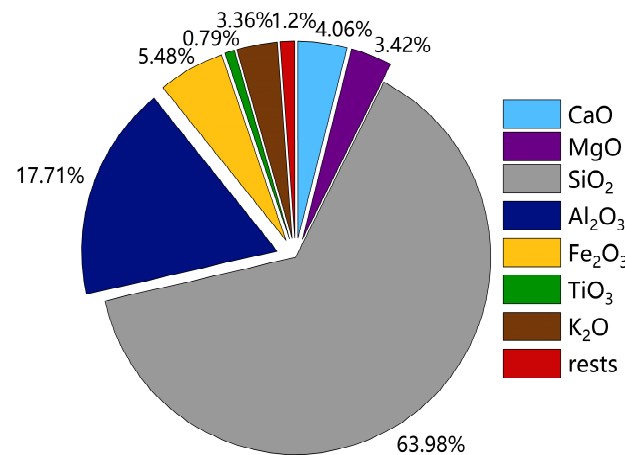
2.1.1. Soil

The soil was collected from a site in Gaomiao Village, Chongqing, with dense soil, small porosity, brownish-red soil color, and large water content, but the soil was still in a plastic state. After bringing the soils back to the laboratory, they were placed into an electric constant temperature air blast drying box to dry and left at 100 °C for 24 h before all steps. Then, they were crushed and passed through a 1 mm nylon sieve after removing stones, tree roots, and other impurities.

Table 1 shows the basic physical properties of soil taken from the limit moisture content test, and the compaction test, which were carried out according to the Standards for Geotechnical Test Methods (GB/T 50123-2019). The soil was sieved to obtain a coarse-grained group containing more than 25% and not more than 50% and satisfying $w_L < 50\%$, $I_p \geq 7$, and $I_p \geq 0.73(w_L - 20)$. According to the engineering classification standard of soil (GB/T 50145-2007), the soil is low-liquid-limit clay. The sealed soil was assessed using the XRF to identify the chemical composition and relative content of each composition. The results are shown in Figure 1.

Table 1. Basic physical properties of undisturbed soil samples.

Physical Property Index	Soil Sample
Liquid Limit/%	27
Plastic Limit/%	12
Plasticity Index (Ip)	15
Optimum Moisture Content/%	11.8
Maximum dry density/g/cm ³	1.91

**Figure 1.** Main chemical components of undisturbed soil.

2.1.2. Binders

Cement, lime, and fly ash were used simultaneously in this study for the following three reasons. (1) Cement costs a lot of energy and releases a lot of carbon according to previous studies [45,46]. Therefore, the use of cement should be reduced; (2) the active substances in fly ash and lime react with the hydration products of cement to further improve properties of the soil and enhance the S/S effects of the HMs; (3) fly ash, as a kind of industrial byproduct, used in this way can reduce the pressure of waste treatment.

Figure 2 shows the results of the X-ray fluorescence analysis of cement, lime, and fly ash, containing the chemical composition and content of each component of three binders. Analytical-grade calcium oxide is the main component of quicklime, which was tested as high as 88.73 percent; the model of the ordinary Portland cement was 325; the fly ash was taken from the Chongqing power plant, and the grade of it was determined as two, according to GB/T 1594-2017. To ensure the uniform mixing of binders and soil, the binders needed to pass a 200-mesh sieve before use.

2.1.3. Heavy Metals

To minimize the influence of anions of the added HM compounds on the test results, analytical-grade $\text{Zn}(\text{NO}_3)_2 \cdot 6\text{H}_2\text{O}$, analytical-grade $\text{Pb}(\text{NO}_3)_2$, and high-purity $\text{Cd}(\text{NO}_3)_2 \cdot 4\text{H}_2\text{O}$ were used simultaneously as HM contaminants to provide the required HM ions. Reactions are difficult to take place between binders, hydration products, and nitrate, while the concentration of nitrate was not high in this research. The side effects of $\text{Zn}(\text{NO}_3)_2 \cdot 6\text{H}_2\text{O}$, $\text{Pb}(\text{NO}_3)_2$, and $\text{Cd}(\text{NO}_3)_2 \cdot 4\text{H}_2\text{O}$ were, thus, negligible [47,48].

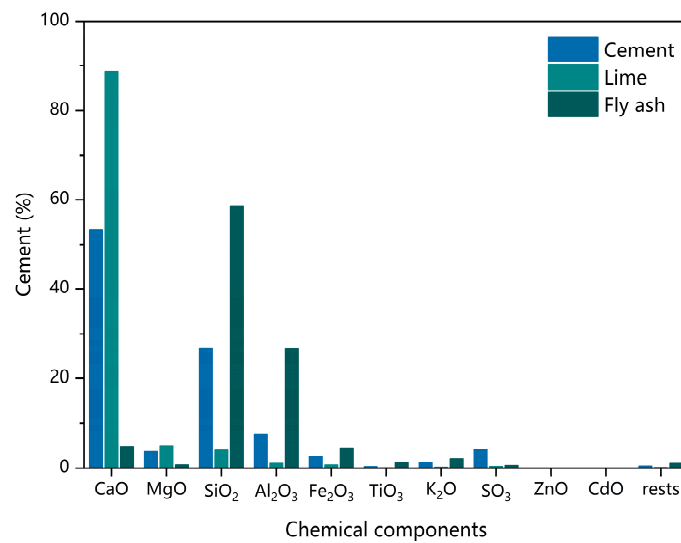


Figure 2. The chemical components of three binders.

2.2. Specimen Preparation

2.2.1. Preparation of Artificial Composite Contaminated Soil

In order to improve the observability of ion changes with F–T cycles in this study, as well as to make the test soils more closely resemble the form of contamination in the project, the tertiary standard limits of Pb, Zn, and Cd in the Soil Environmental Quality Standard (GB36000-2018) were enlarged by 16, 10, and 400 times, respectively, to obtain test yields of 8000 mg/kg, 5000 mg/kg, and 400 mg/kg for Pb, Zn and Cd, respectively.

At the same time, the soil moisture content was set at 120% of the optimal moisture content to ensure adequate F–T effects, and then, according to the soil water content and the HM mixture, a certain amount of deionized water, analytical-grade $\text{Pb}(\text{NO}_3)_2$, analytical-grade $\text{Zn}(\text{NO}_3)_2 \cdot 6\text{H}_2\text{O}$, and high-purity $\text{Cd}(\text{NO}_3)_2 \cdot 4\text{H}_2\text{O}$ was weighed and placed in a magnetic mixer for ten minutes to mix the solution well.

After that, the mixed solution was added to the sieved soil, stirred with a magnetic mixer for 10 min, then wrapped in a plastic bag and placed in a humidor with a temperature of 22 °C and a relative humidity of 95% for 30 days to make an artificial composite HMs-contaminated soil.

2.2.2. Stabilization/Solidification of Contaminated Soil

According to the previous results of our research group [41], the better designed mixing ratio of cement, lime, and fly ash on S/S of HMs-contaminated soil is 5%, 2.5%, and 2.5%, respectively, so this ratio was adopted in our current study. After weighing a certain amount of binder according to the binders' set ratio, the soil-added binders were stirred by a mechanical mixer for 10 min, then sealed by a plastic membrane and kept for 56 days in a standard curing chamber (22 °C, 95% relative humidity) for use.

2.3. Testing Methods

2.3.1. Freeze–Thaw Test

The alternately high- and low-temperature test chamber (Chongqing Tester Experimental Instrument Co., Ltd. Chongqing, China) is the instrument for F–T tests. Five kinds of F–T cycles were designed for the specimens, including 3, 7, 14, 30, and 90 F–T cycles (0 F–T cycle was set as the control group). The setting mode of one cycle is shown in Table 2 (24 h for each cycle), in which the freezing temperature of the soil was set at −10 °C, and the dissolution temperature was 20 °C. To ensure the complete freezing and dissolution of the soil, it was maintained for 11 h after reaching the specified temperature. The F–T cycled specimens were ground and pounded through a 200-mesh sieve to meet the experimental.

Table 2. The form of the F–T cycles.

Temperature Form	From 20° to – 10°	Remaining – 10°	From – 10° to 20°	Remaining 20°
Time/h	0–1	2–12	12–13	14–24

Note: The first time the soil freezes, it starts to drop from room temperature.

2.3.2. The Improved Tessier Method

According to the Geological Survey Standards of China Geological Bureau (DD2005-03), the improved Tessier method was adopted to determine the distribution of seven fractions of three HMs of S/S Pb–Zn–Cd HM-contaminated soil under six conditions. This method is to further divide the organically bound fractions in the Tessier sequential extraction method proposed by Tessier into strongly organically bound fractions and humic-acid-bound fractions, and additionally add the water-soluble fraction [49,50]. The seven forms in the method are water-soluble fraction, ion exchange fraction, carbonate-bound fraction, iron and manganese oxidation fraction, weak organic fraction, strong organic fraction, and residue fraction.

The main reagents used are as follows, according to Technical Standards for Geological Survey of China Geological Survey (DD2005-03).

- (a) Hydrochloric acid ($\rho(\text{HCl}) = 1.18 \text{ g/mL}$);
- (b) Hydrochloric acid in which concentrated hydrochloric acid and water are mixed in a volume ratio of 1:1;
- (c) Nitric acid ($\rho(\text{HNO}_3) = 1.41 \text{ g/mL}$);
- (d) Nitric acid ($c(\text{HNO}_3) = 0.02 \text{ mol/L}$);
- (e) Perchlorate ($\rho(\text{HClO}_4) = 1.66 \text{ g/mL}$);
- (f) Hydrofluoric acid ($\rho(\text{HF}) = 1.15 \text{ g/mL}$);
- (g) Magnesium chloride ($c(\text{MgCl}_2 \cdot 6\text{H}_2\text{O}) = 1.0 \text{ mol/L}$, $\text{pH} = 7.0 \pm 0.2$)

Five hundred and eight grams $\text{MgCl}_2 \cdot 6\text{H}_2\text{O}$ was weighed and dissolved in distilled water in a 2500 mL plastic bucket. The pH was adjusted by NaOH ($\omega(\text{NaOH}) = 10\%$).

- (h) Sodium acetate ($c(\text{CH}_3\text{COONa} \cdot 3\text{H}_2\text{O}) = 1.0 \text{ mol/L}$, $\text{pH} = 5 \pm 0.2$)

Three hundred and forty grams $\text{CH}_3\text{COONa} \cdot 3\text{H}_2\text{O}$ was weighed and dissolved in distilled water in a 2500 mL plastic bucket. The pH was adjusted by CH_3COOH .

- (i) Sodium pyrophosphate ($c(\text{Na}_4\text{P}_2\text{O}_7 \cdot 10\text{H}_2\text{O}) = 0.1 \text{ mol/L}$, $\text{pH} = 10.0 \pm 0.2$)

One hundred and eleven and a half grams $\text{Na}_4\text{P}_2\text{O}_7 \cdot 10\text{H}_2\text{O}$ was weighed and dissolved in distilled water in a 2500 mL plastic bucket, and the pH was adjusted to 10.0 ± 0.2 with HNO_3 where concentrated nitric acid and water are mixed in a volume ratio of 1:1.

- (j) Ammonium hydroxide hydrochloride–hydrochloric acid mixture ($c(\text{HONH}_3\text{Cl}) = 0.25 \text{ mol/L}$, $c(\text{HCl}) = 0.25 \text{ mol/L}$)

Forty-three point four grams HONH_3Cl was weighed and 104 mL hydrochloric acid was added, where concentrated hydrochloric acid and water are mixed in a volume ratio of 1:1 and dissolved in distilled water in a 2500 mL plastic bucket.

- (k) Hydrogen peroxide ($\varphi(\text{H}_2\text{O}_2) = 30\%$, $\text{pH} = 2.0 \pm 0.2$)

The pH was adjusted by nitric acid where concentrated nitric acid and water are mixed in a volume ratio of 1:1.

- (l) Ammonium acetate–nitric acid mixture ($c(\text{CH}_3\text{COONH}_4) = 3.2 \text{ mol/L}$, $c(\text{HNO}_3) = 4.48 \text{ mol/L}$)

Six hundred and sixteen point six grams $\text{CH}_3\text{COONH}_4$ was weighed and added 500 mL HNO_3 (c). Both were dissolved in a 2500 mL plastic bucket with distilled water.

Using the above reagent, the concentration of HMs in soil under seven forms could be accurately determined according to the following nine steps.

- (1) A sample of 2.5000 g was accurately weighed and placed in a centrifuge tube.
- (2) Extraction of water-soluble fraction.

Distilled water was used as the extraction agent for water-soluble HMs. First, 25 mL of distilled water was added to the beaker and shaken well, then the beaker was placed into the ultrasonic cleaner. Ultrasound was performed at the working mode of 5 min with 5 min intervals at a frequency of 40 kHz, and the total working time was 30 min, during which the water temperature in the ultrasonic cleaner was 25 ± 5 °C. Then, the material in the beaker was transferred into a centrifuge tube for centrifugation (20 min at a speed of 4000 r/min), the precipitated supernatant was filtered with a pore diameter of 0.45 µm, and then the liquid was poured into a 25 mL colorimetric tube. An Optima 8000 inductively coupled plasma emission spectrometer was used to detect the contents of lead, zinc, and cadmium in the extracted liquid.

- (3) Residue cleaning

The remaining residue was added to about 100 mL distilled water to wash the precipitation, and centrifuged at 4000 r/min for 10 min. The aqueous phase was discarded, and the residue was left.

- (4) Extraction of ion-exchange fraction

Twenty-five milliliters of magnesium chloride (g) solution were accurately added to the residue left in step (3), shaken well, and placed in an ultrasonic cleaner that had been placed into water. Ultrasound was performed at a frequency of 40 kHz for 30 min (ultrasonic was performed for 5 min every 5 min during this period, and the water temperature in the ultrasonic cleaner was controlled at 25 ± 5 °C). After the ultrasound, they were taken out, and centrifuged at 4000 r/min for 20 min. A total of 5 mL of liquid was taken into a 10 mL colorimetric tube and added to 0.5 mL of hydrochloric acid (a). After that, the distilled water was used for constant volume to scale. After shaking the colorimetric tube well, the ICP-OES theory was used to determine the content of HMs in liquid. The step of residue cleaning was repeated at last.

- (5) Extraction of carbonate-bound fraction

Sodium acetate (h) was selected as the extraction agent of carbonate-bound fraction. A total of 25 mL of it was added to the residue which came from step (4), shaken well, and placed in an ultrasonic cleaner with a frequency of 40 kHz for 1 h (ultrasonic was performed for 5 min every 5 min during the period, and the water temperature in the ultrasonic cleaner was controlled at 25 ± 5 °C). Then they were taken out and centrifuged at 4000 r/min for 20 min. Separated 5 mL liquid was poured into a 10 mL colorimetric tube. After adding 0.5 mL HCl (a) to the colorimetric tube, the distilled water was brought to scale, and shaken well. An Optima 8000 inductively coupled plasma emission spectrometer was used to analyze the contents of lead, zinc, and cadmium, and step (3) was repeated finally.

- (6) Extraction of humic-acid-bound fraction

Fifty milliliters sodium pyrophosphate solution (i) was accurately added to the residue obtained in step (5). After shaking well, it was taken to the ultrasonic cleaner with a frequency of 40 kHz for 40 min (ultrasonic 5 min every 5 min during this period, and the water temperature in an ultrasonic cleaner is controlled at 25 ± 5 °C) and placed for 2 h. Then, the solution was centrifuged at 4000 r/min for 20 min. A 50 mL beaker was filled with 10 mL clear liquid and 5 mL HNO₃ (c) and 1.5 mL HClO₄ were added (e). The surface dish was used to cover the beaker, and the beaker was heated and steamed on the electric heating plate until the occurrence of HClO₄ white smoke exhaust. Then, 1 mL HCl (b) was added, the surface dish was washed, and the dissolved salt was heated, removed, and cooled. Finally, a 10 mL colorimetric tube was scaled by distilled water. After shaking well, an Optima 8000 inductively coupled plasma emission spectrometer was used to analyze the contents of lead, zinc, and cadmium. The remaining residue was treated as described in step (3).

(7) Extraction of iron and manganese oxidized bond fraction

Fifty milliliters hydroxylamine hydrochloride solution (j) was added to residue obtained from step (6) accurately. After they were shaken well, the ultrasound was carried out in ultrasonic cleaner with a frequency of 40 kHz for 1 h (ultrasonic for 5 min every 5 min during this period, water temperature in an ultrasonic cleaner is controlled at 25 ± 5 °C). Then, the solution was removed and centrifuged at 4000 r/min for 20 min. Finally, 10 mL clear liquid was separated into a colorimetric tube. The contents of lead, zinc, and cadmium were analyzed by the ICP-OES method. The remaining precipitation was transferred to a 50 mL centrifuge tube with 50 mL distilled water and centrifuged for 10 min at a speed of 4000 r/min. The aqueous phase was discarded, and the residue was left after cleaning twice.

(8) Extraction of strong organic bonding fraction

Three milliliters HNO_3 (d) and 5 mL H_2O_2 (k) were accurately added to the residue obtained from step (7). The solution was shaken well and kept for 1.5 h in a constant temperature water bath at 83 ± 3 °C (stirred once every 10 min during the period). Then, the solution was continued to have 3 mL H_2O_2 added (k) and kept warm in the water bath for 1 h and 10 min (stirring once every 10 min during this period). After cooling to room temperature, 2.5 mL ammonium acetate–nitric acid solution (a) was added, and the samples were diluted to about 25 mL and stirred for 1 min, then placed at 25 ± 5 °C overnight, and centrifuged at 4000 r/min for 20 min. The clear liquid was poured into a 50 mL colorimetric tube, diluted with distilled water to scale, and shaken well. Then, a 50 mL beaker was used. First, 25 mL separated clear liquid, 10 mL HNO_3 (c), and 1 mL HClO_4 (e) was poured in, then, with a surface dish, it was heated on the electric heating plate at low temperature until it was nearly dry, and at high temperature until the concentrated white smoke was cleared. After this, 5 mL HCl (b) was added while hot, and the dish was washed. The beaker was heated at a low temperature until the salts dissolved. After the solution cooled, 25 mL of water was placed into a colorimetric tube and shaken well. A 5 mL solution was separated into 10 mL colorimetric tubes for ICP-OES analysis for Pb, Zn, and Cd. About 20 mL of distilled water was added to wash the sediment, and centrifuged for 10 min at a speed of 4000 r/min. The aqueous phase was discarded. The cleaning process was carried out twice, leaving the residue at the end.

(9) Extraction of residue fraction

The cleaned residue obtained from step (8) was air-dried, ground, weighed, and the correction factor was calculated, and then the sample of 0.2000 g was accurately taken out and placed in the PTFE crucible. The sample was wetted in the crucible by water and 5 mL of hydrochloric acid (f), nitric acid, and perchloric acid mixture in the ratio of 1:1:1 was added. The crucible was heated on an electric heating plate until the white smoke of perchloric acid was fully distributed. Then, 3 mL of hydrochloric acid (b) was added to the crucible. After the crucible wall was washed, the crucible continued to heat until the salt was dissolved, and then cooled to room temperature. Finally, the remaining product was transferred to a colorimetric tube, and the volume was kept at 25 mL and shaken well. The contents of lead, zinc, and cadmium were analyzed by the ICP-OES method.

2.3.3. Fourier Transform Infrared Spectrum (FTIR) Analysis Test

The attenuated total reflection Fourier transform infrared spectroscopy method was adopted in this study. Six kinds of soil were dried at 100 °C for 24 h and tested by a Fourier infrared spectrometer after passing through a 200-mesh sieve. The mid-infrared region was used for detection in this study. The following procedures were used to analyze the spectrum [51].

The measured mid-infrared was tentatively divided into a characteristic functional group area ($4000\text{--}1333\text{ cm}^{-1}$) and a fingerprint area ($1333\text{--}400\text{ cm}^{-1}$), then the characteristic functional group was further divided into three wavebands ($4000\text{--}2400\text{ cm}^{-1}$, $2400\text{--}2000\text{ cm}^{-1}$, and $900\text{--}400\text{ cm}^{-1}$), and the fingerprint area was finely divided into two wavebands ($1333\text{--}900\text{ cm}^{-1}$ and $900\text{--}400\text{ cm}^{-1}$). Infrared spectroscopies were taken as a preliminary analysis (compound type, functional group, the structural unit, etc.) based on the corresponding characteristic absorption bands to determine the possible functional groups and possible structural units.

Based on possible functional groups, possible structural units, the characteristic frequency table of the characteristic absorption bands of various compounds, and various factors affecting the movement of characteristic frequencies, the structural details were revealed. The standard spectra of related compounds determined according to the details were compared with the obtained spectra of soils under six environments to obtain specific functional group composition.

3. Results

3.1. Effect of Solidification/Stabilization on the Speciation of Different Heavy Metals

Among the seven different HM fractions extracted by the improved Tessier method, the order of bioavailability for different fractions of HMs in the soil is shown as follows: water-soluble state > ion-exchange state > carbonate-bound fraction > humic-acid-bound fraction > iron and manganese oxidized bond fraction > strong organic bonding fraction > residue fraction. Pb^{2+} , Zn^{2+} , and Cd^{2+} provided by $\text{Pb}(\text{NO}_3)_2$, $\text{Zn}(\text{NO}_3)_2 \cdot 6\text{H}_2\text{O}$, and $\text{Cd}(\text{NO}_3)_2 \cdot 4\text{H}_2\text{O}$ are in the ion exchange fraction. HMs whose bioavailability is greater than this form can be considered to have undergone a transition to the stable forms, and are referred to as the stable form, while the ion-exchange fraction and the water-soluble fraction are set as the unstable form.

Figure 3 shows the relative content of HMs in the S/S soil under a non-freeze–thaw condition in the unstable fraction, and the stable fraction. It is obvious that the content of Pb ion, Zn ion, and Cd ion supplied in the soil decreased sharply after the S/S by adding cement, lime, and fly ash. After S/S, the unstable forms of Pb, Zn, and Cd remain as only 1.19%, 1.09%, and 24.89%, respectively.

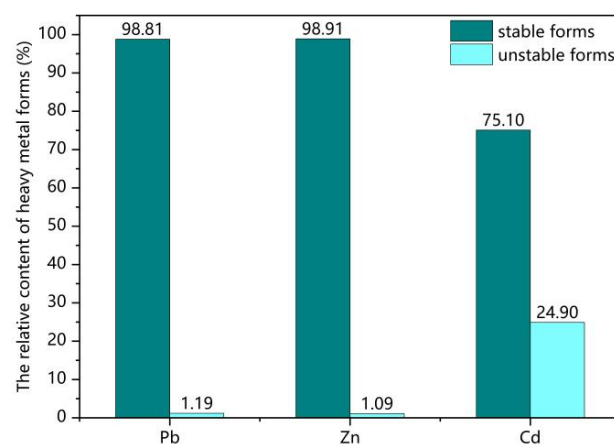


Figure 3. The relative content of heavy metals (HMs) in the solidified/stabilized (S/S) Pb–Zn–Cd composite HM-contaminated soil without F–T cycles.

However, Figure 3 also shows that the S/S efficiency varies for different HMs. The relative contents of the stable forms of Pb and Zn are much larger than that of the stable fractions of Cd. After the S/S process, 98.81% of lead and 98.91% of zinc were converted to a stable fraction, but only 75.10% of cadmium was converted to a stable fraction, with a relative content difference of more than 20%.

3.2. Effect of F–T Cycles on the Speciation of HMs

Figure 4 reveals the trend of the relative content of the two types of fractions of HMs in the S/S Pb–Zn–Cd composite HM-contaminated soil with the action of F–T cycles. The changing trend of the curve in it indicates that the F–T cycle causes HMs to transform from stable to unstable forms, but the reduction of stable HM becomes slow after reaching 14 cycles. After 90 F–T cycles, the relative contents of stable forms of Pb, Zn, and Cd in the soil decreased by 1.27%, 3.11%, and 8.16%, respectively, while the decrease reached more than 50% of the total decrease after 14 F–T cycles.

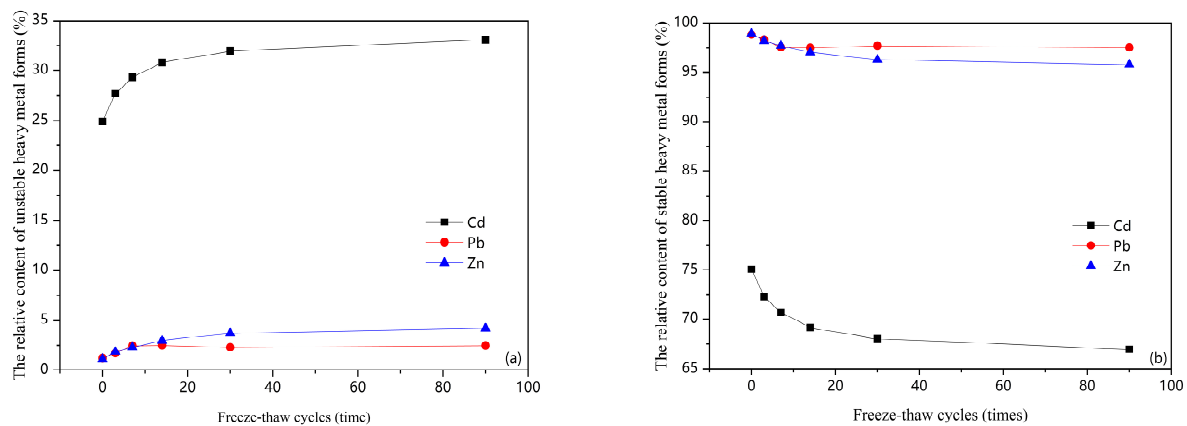


Figure 4. The variation of the relative content of HM forms with F–T cycles in the S/S Pb–Zn–Cd composite HM-contaminated soil. (a) unstable HM forms; (b) stable HM forms.

The variation of the relative content of stable fractions of three HMs in S/S soil with the number of F–T cycles is shown in Figure 5. It can be seen that the relative content of the carbonate-bound fraction of HMs decreases significantly with F–T cycles. The effect is significant within the 14 F–T cycles, the slope of the curve is large, and the rate of decline is fast. However, with the increase of the F–T cycles times, the rate of decline of carbonate-bound forms becomes relatively slow. After 14 F–T cycles, the relative contents of carbonate-bound fraction of Pb, Zn, and Cd decreased by 13.46%, 7.35%, and 8.68%, respectively, while the relative contents of corresponding types only decreased by 2.06% in the process from 14 F–T cycles to 90 F–T cycles, 4.58%, and 1.56%.

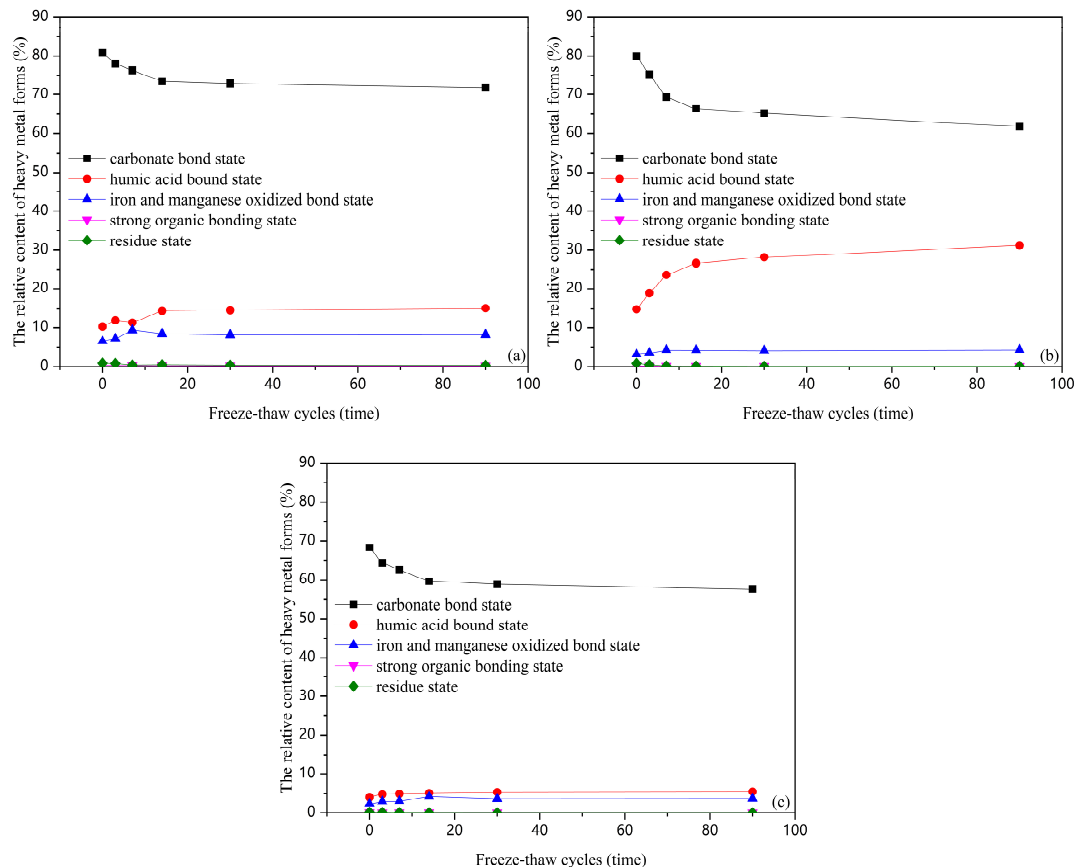


Figure 5. The variation of relative content of each speciation of HMs with F–T cycles in the S/S Pb–Zn–Cd composite HM-contaminated soil. (a) Zn; (b) Pb; (c) Cd.

3.3. Effect of F–T Cycles on the Functional Groups in S/S Soil

Figure 6 shows the FTIR spectra of S/S Pb–Zn–Cd composite HM-contaminated soil under six F–T cycle conditions (0, 3, 7, 14, 30, and 90 cycles). According to their own spectra, a large amount of literature data, and standard Fourier infrared spectrogram, the types of functional groups in each condition were distinguished.

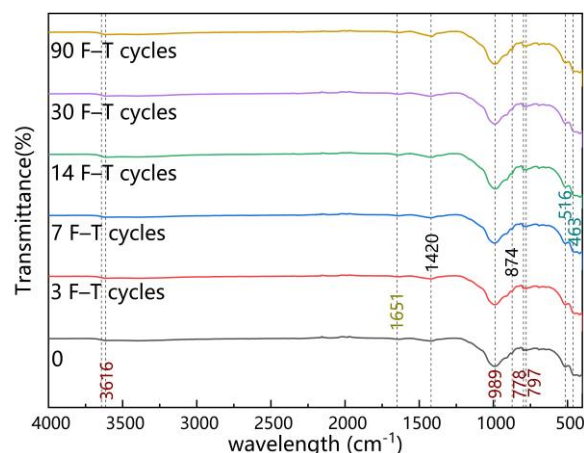


Figure 6. FTIR spectra of S/S Pb–Zn–Cd composite HMs-contaminated soil under 6 F–T cycle conditions (0, 3, 7, 14, 30, and 90 cycles).

The locations of the characteristic peaks of the FTIR spectra under the six F–T conditions are roughly the same, indicating that within 90 F–T cycles, the types of target substances (soil components, binder components, hydration products, etc.) detected in the S/S Pb–Zn–Cd composite HMs-contaminated soil did not change.

Seven hundred and ninety-seven per centimeter, and Seven hundred and eighty-seven per centimeter are caused by Si–O–Si stretching vibrations, which are typical double peaks of quartz minerals, which is an important part of the soil itself, and the added binders. The peaks at 516 cm^{-1} and 463 cm^{-1} are the Si–O vibration absorption peaks of the gel [52,53]. There are two main reasons for the existence of the characteristic peak of colloid. One is that the effective component of cement, tricalcium silicate, and dicalcium silicate, generates a large amount of hydrated calcium silicate colloid after hydration; the other is that the hydration product of cement, calcium hydroxide, continues to react with lime and fly ash to form colloids [54]; among them, there was residual calcium hydroxide, and the characteristic peak appears in 1651 cm^{-1} . The existence of colloids has made a great contribution to the S/S of HMs, such as the large amounts of adsorption of HM ions, and the filling of soil pores, which hinders the flow of HMs. The formation of calcium hydroxide also underwent a substitution reaction with HM ions, causing HM ions to precipitate.

Eight hundred and seventy-four per centimeter and one thousand four hundred and twenty per centimeter are caused by carbonate stretching vibration. These two obvious characteristic peaks appeared in the FTIR spectra under every F–T condition (0, 3, 7, 14, 30, and 90 F–T cycles). This is mainly produced by the entry of carbon dioxide into the atmosphere and is affected by the pH of the soil. There is a huge relationship with the formation of HM carbonate-bound fraction.

4. Discussion

4.1. Effect of Solidification/Stabilization on the Speciation of Different Heavy Metals

The results in Section 3.1 show the transfer of HMs to stable forms after the addition of binders. After the hydration reaction of the binders, their hydration products will interact with HMs, increasing the inertness of HMs and reducing the migration ability of HMs.

The first mechanism for immobilization of HMs is a chemical reaction, in which lead, zinc, and cadmium react with $\text{Ca}(\text{OH})_2$, calcium silicate hydrates, and so on, and are fixed

to the binder components. Furthermore, the S/S technology also has a certain physical effect on the treatment process of HMs through the improvement of soil properties and the progress of the chemical reaction of the binders [55]. The decrease in soil permeability will hinder the migration of HMs, and the colloids produced by the curing agent will physically encapsulate the HMs [56]. Soil S/S technology, as a risk management technology, has a strong effect on reducing the risk of HMs. However, it can be clearly found that for different HMs in the soil, the conversion efficiency is different, with cadmium having the lowest conversion efficiency, with a difference of 20% compared to the other two HMs. The factors causing this phenomenon may have the following three aspects.

First, the properties of each HM are different [55]. Compared with cadmium ions, lead ions are more electronegative and have poor reaction activity [57]. Second, the S/S of HMs is closely related to the pH value of the soil, and different kinds of HM have different optimal pH values for S/S [58–60]. Most lead ions precipitate at a pH of about 9.8 and remain stable within a pH of 12 [61]. Zinc hydroxide begins to precipitate when pH is above 5 [62], and crystalline $\text{Cd}(\text{OH})_2$ is precipitated in soil when pH is increased to above 6.2 [63]. Finally, the initial content of the three elements added to the undisturbed soil is different, the added cadmium is the least, and the progress of S/S will be less targeted.

4.2. Effect of F–T Cycles on the Speciation of HMs

The main reasons for this phenomenon are as follows. Through the continuous action of the F–T cycle, the porosity ratio in the soil keeps increasing, making it easier for carbon dioxide to enter the soil. Some studies have shown that the carbonization process of soil has adverse effects on the S/S of HMs. The pH value of the soil keeps decreasing with the carbonization, causing hydrolysis of the hydration products of many adhesives, and further activation of more HMs.

This is due to the fact that the carbonate-bound fraction of HMs is very sensitive to the change of pH. Under alkaline conditions, the carbonate-bound fraction is relatively stable. With the continuous decrease of soil pH under the action of the F–T cycle, the HM compounds in the carbonate-bound fraction decompose, while the rate of decomposition is associated with the change speed of pH because the degree of influence of carbon dioxide on soil Ph gradually decreases over time. During this time, the process of S/S of HM is still underway but does not play a dominant role.

As the F–T cycle progresses, the relative content of the humic-acid-bound fraction, iron and manganese oxidized bond fraction, strong organic bonding fraction, and residue fraction in the stable form increases continuously. However, due to their small content, they have little influence on the overall fraction of HMs, so the relative content of the stable form of HMs is still in a downward trend as the F–T cycle progresses. It may also be noted that these four HM forms are not sensitive to pH.

4.3. Effect of F–T Cycles on the Functional Groups in S/S Soil

According to Figure 6, a large number of Si–O–Si stretching vibrations, Si–O vibration absorption peaks, and carbonate stretching vibration can be found in the sample; this proves that substances that can enhance the stability of HMs, such as colloids and carbonate binders, are indeed present in the soil at this time [52,53]. This is why a large number of HMs have previously undergone a transition to the steady fractions.

Meanwhile, the types of functional groups contained in the soil are approximately the same in the six cases. The direct effect of the F–T cycle on the soil is mainly a physical reaction without the addition of new substances; therefore, the number of characteristic peaks did not increase. Meanwhile, the result of chemical speciation analysis shows that when the number of F–T cycles exceeded 14 times, the changing trend of the content of each HM forms was very slow, and gradually stabilized instead of a single decline. Therefore, there was no disappearance of the characteristic peak. Due to the above reasons, the F–T cycle did not change the types of functional groups in the system.

In addition, carbonate stretching vibration was detected in the soil. This is consistent with the fact that there are carbonate binders in the soil, and that when the pH environment in which the HMs are located changes, the HMs react with the carbonates to varying degrees. The F–T cycles, on the other hand, increase the amount of carbon dioxide entering the soil precisely by changing the porosity of the soil, causing changes in the carbonate-bound fraction of the soil.

Throughout the whole process of this study, it is clearly recognized that the change in the content of its stable fractions tends to slow down when the F–T cycles are performed several times. According to the experimental results, this node occurs at 30 cycles. When conducting an HM soil remediation project, the collected soil samples can be S/S in the laboratory and then subjected to a small trial test of 30 F–T cycles to test the morphological components, derive the instability limits, determine whether there is a safety hazard, and determine whether to keep the curing ratios or change the curing ratios.

5. Conclusions

The improved Tessier method and Fourier transform infrared spectrum (FTIR) analysis test were used to study the effects of long-term F–T on the S/S of Pb–Zn–Cd composite HM-contaminated soil in this study. The soil morphology and FTIR spectra were tested in six environments (without F–T cycles, with 3 cycles, 7 cycles, 14 cycles, 30 cycles, and 90 cycles) in HM-contaminated soil, and the following remarkable conclusions were obtained.

In the S/S Pb–Zn–Cd composite HM-contaminated soil, the addition of three binders, cement, lime, and fly ash, reduces the HM risk by making HMs exist in a more stable form. The characteristic peaks at 463 cm^{-1} and 516 cm^{-1} of the FTIR spectra indicate the presence of colloids that can adsorb and store HMs, and the characteristic peak of calcium hydroxide that can precipitate HMs appeared at 1651 cm^{-1} . However, for different types of HMs, the S/S efficiency is different. The relative content of HMs transferred to stable forms in lead and zinc is 20% greater than that in cadmium.

The content of HMs in a steady state decreased continuously with the increase of frequency of F–T cycles. There were drastic changes before 14 cycles, but with the continuous increase in the frequency of F–T cycles, the increasing trend gradually decreases, and the rate of decrease in the stable form of HMs became minimal after 30 F–T cycles. This is the main reason why F–T cycles would not change the types of functional groups.

Under the action of long-term F–T cycles, the decrease in the stable form content of HMs in the S/S composite HM-contaminated soil is mainly caused by the decrease in the carbonate-bound state content. Its peaks appeared at 874 cm^{-1} and 1420 cm^{-1} . Ninety F–T cycles caused the carbonate-bound content of Pb, Zn, and Cd to decrease by 18.04%, 8.92%, and 10.74%, respectively.

Through this experiment, it can be seen that after the number of F–T cycles reaches 30, the decrease rate of stable form HM content reaches the minimum; therefore, 30 F–T cycles can be used as the critical test point for indoor tests in actual projects to determine the danger zone. However, for different soils, exactly how the critical number changes is not yet known; in future research, it is recommended that the majority of scholars conduct further research on this part. At the same time, the huge change in the content of the carbonate-bound fraction of HMs during the F–T cycles must also recognize the tremendous influence of environmental pH on the S/S effect, and numerous studies have been conducted by domestic and foreign scholars on this content in the hope that a risk control method for the common assessment of various influencing factors can be established in the future.

Author Contributions: Conceptualization, Z.Y.; methodology, Z.Y. and Y.W.; investigation, Y.W., X.L., J.C. and K.Z.; writing—original draft preparation, J.C.; writing—review and editing, Z.Y.; supervision, Z.Y., X.L. and K.Z. All authors have read and agreed to the published version of the manuscript.

Funding: This research was funded by the National Natural Science Foundation of China, grant number 42177125 and the National Natural Science Foundation of China, grant number 41772306.

Institutional Review Board Statement: Not applicable.

Informed Consent Statement: Not applicable.

Data Availability Statement: Not applicable.

Acknowledgments: The authors acknowledge the financial support received from the National Natural Science Foundation of China (Grant No. 42177125, and No. 41772306). We also thank Ren Shupe and Wang Yao, graduate students, for their efforts in terms of conducting the laboratory tests.

Conflicts of Interest: The authors declare no conflict of interest. The funders had no role in the design of the study; in the collection, analyses, or interpretation of data; in the writing of the manuscript, or in the decision to publish the results.

References

1. Xue, Q.; Zhan, L.T.; Hu, L.M.; Du, Y.J. Environmental geotechnics: State-of-the-art of theory, testing and application to practice. *China Civil. Eng. J.* **2020**, *53*, 80–94.
2. Liu, S.Y. Geotechnical investigation and remediation for industrial contaminated sites. *Chin. J. Geotech. Eng.* **2018**, *40*, 1–37.
3. Kogbara, R.B. A review of the mechanical and leaching performance of stabilized/solidified contaminated soils. *Environ. Rev.* **2014**, *22*, 66–86. [[CrossRef](#)]
4. Cao, X.; Ma, R.; Zhang, Q.S.; Wang, W.B.; Liao, Q.X.; Sun, S.C.; Zhang, P.X.; Liu, X.L. The factors influencing sludge incineration residue (SIR)-based magnesium potassium phosphate cement and the solidification/stabilization characteristics and mechanisms of heavy metals. *Chemosphere* **2020**, *261*, 127789. [[CrossRef](#)] [[PubMed](#)]
5. Hao, H.Z.; Chen, T.B.; Jin, M.G.; Lei, M.; Liu, C.W.; Zu, W.P.; Huang, L.M. Recent advance in solidification /stabilization technology for the remediation of heavy metalscontaminated soil. *Chin. J. Appl. Ecol.* **2011**, *22*, 816–824.
6. Zhang, T.T.; Li, J.S.; Wang, P.; Huang, Q.; Xue, Q. Experimental study of mechanical and microstructure properties of magnesium phosphate cement treated lead contaminated soils. *Rock Soil Mech.* **2016**, *37*, 279–286.
7. Ngo, H.T.T.; Watchalayann, P.; Nguyen, D.B.; Doan, H.N.; Liang, L. Environmental health risk assessment of heavy metal exposure among children living in an informal e-waste processing village in Viet Nam. *Sci. Total Environ.* **2021**, *763*, 142982. [[CrossRef](#)]
8. Ustaoglu, F.; Islam, M.S. Potential toxic elements in sediment of some rivers at Giresun, Northeast Turkey: A preliminary assessment for ecotoxicological status and health risk. *Ecol. Indic.* **2020**, *113*, 106237. [[CrossRef](#)]
9. Islam, M.S.; Ahmed, M.K.; Al-Mamun, M.H.; Eaton, D.W. Human and ecological risks of metals in soils under different land-use types in an urban environment of Bangladesh. *Pedosphere* **2020**, *30*, 201–213. [[CrossRef](#)]
10. He, L.Z.; Zhong, H.; Liu, G.X.; Dai, Z.M.; Brookes, P.C.; Xu, J.M. Remediation of heavy metal contaminated soils by biochar: Mechanisms, potential risks and applications in China. *Environ. Pollut.* **2019**, *252*, 846–855. [[CrossRef](#)]
11. Markus, J.; McBratney, A.B. A review of the contamination of soil with lead. *Environ. Int.* **2001**, *27*, 399–411. [[CrossRef](#)]
12. Buddhi, W.; Liu, A.; He, B.B.; Yang, B.; Zhao, X.; Godwin, A. Ashantha G Behaviour of metals in an urban river and the pollution of estuarine environment. *Water Res.* **2019**, *196*, 414911.
13. Shao, Y.Y.; Yan, T.; Wang, K.; Huang, S.M.; Yuan, W.Z.; Qin, F.G.F. Soil heavy metal lead pollution and its stabilization remediation technology. *Energy Rep.* **2020**, *6*, 122–127. [[CrossRef](#)]
14. Liu, S.J.; Miao, C.; Yao, S.S.; Ding, H.; Zhang, K. Soil stabilization/solidification (S/S) agent-water-soluble thiourea formaldehyde (WTF) resin: Mechanism and performance with cadmium. *Environ. Pollut.* **2021**, *272*, 116025. [[CrossRef](#)]
15. Gong, Y.Y.; Zhao, D.Y.; Wang, Q.L. An overview of field-scale studies on remediation of soil contaminated with heavy metals and metalloids: Technical progress over the last decade. *Water Res.* **2018**, *147*, 440–460. [[CrossRef](#)]
16. Qin, C.C.; Yuan, X.Z.; Xiong, T.; Tan, Y.Z.; Wang, H. Physicochemical properties, metal availability and bacterial community structure in heavy metal-polluted soil remediated by montmorillonite-based amendments. *Chemosphere* **2020**, *261*, 128010. [[CrossRef](#)]
17. Gao, P.; Yue, S.J.; Chen, H.T. Carbon emission efficiency of China's industry sectors: From the perspective of embodied carbon emissions. *J. Clean. Prod.* **2021**, *283*, 124655. [[CrossRef](#)]
18. Yang, Z.P.; Wang, Y.; Li, D.H.; Li, X.Y.; Liu, X.R. Influence of Freeze–Thaw Cycles and Binder Dosage on the Engineering Properties of Compound Solidified/Stabilized Lead-Contaminated Soils. *Int. J. Environ. Res. Public Health* **2020**, *17*, 1077. [[CrossRef](#)]
19. Wang, F.; Pan, H.; Xu, J. Evaluation of red mud based binder for the immobilization of copper, lead and zinc. *Environ. Pollut.* **2020**, *263*, 114416. [[CrossRef](#)]
20. Bai, B.; Rao, D.Y.; Chang, T.; Guo, Z.G. A nonlinear attachment-detachment model with adsorption hysteresis for suspension-colloidal transport in porous media. *J. Hydrol.* **2019**, *587*, 124080. [[CrossRef](#)]
21. Zha, F.S.; Zhu, F.H.; Xu, L.; Kang, B.; Yang, C.B.; Zhang, W.; Zhang, J.W.; Liu, Z.H. Laboratory study of strength, leaching, and electrical resistivity characteristics of heavy-metal contaminated soil. *Environ. Earth Sci.* **2021**, *80*, 184. [[CrossRef](#)]
22. Zha, F.S.; Qiao, B.R.; Kang, B.; Xu, L.; Chu, C.F.; Yang, C.B. Engineering properties of expansive soil stabilized by physically amended titanium gypsum. *Constr. Build. Mater.* **2021**, *303*, 124456. [[CrossRef](#)]
23. Wang, F.; Xu, J.; Yin, H.L.; Zhang, Y.H.; Pan, H.; Wang, L. Sustainable stabilization/solidification of the Pb, Zn, and Cd contaminated soil by red mud-derived binders. *Environ. Pollut.* **2021**, *284*, 117178. [[CrossRef](#)] [[PubMed](#)]

24. Bai, B.; Zhou, R.; Cai, G.Q.; Hu, W.; Yang, G.C. Coupled thermo-hydro-mechanical mechanism in view of the soil particle rearrangement of granular thermodynamics. *Comput. Geotech.* **2021**, *137*, 104272. [[CrossRef](#)]
25. Zha, F.S.; Liu, C.M.; Kang, B.; Xu, L.; Yang, C.B.; Chu, C.F.; Yu, C.; Zhang, W.; Zhang, J.W.; Liu, Z.H. Effect of Carbonation on the Leachability of Solidified/Stabilized Lead-Contaminated Expansive Soil. *Adv. Civil. Eng.* **2021**, *2021*, 8880818. [[CrossRef](#)]
26. Du, Y.J.; Jiang, N.J.; Shen, S.L.; Jin, F. Experimental investigation of influence of acid rain on leaching and hydraulic characteristics of cement-based solidified/stabilized lead contaminated clay. *J. Hazard. Mater.* **2012**, *225*, 195–201. [[CrossRef](#)]
27. Du, Y.J.; Wei, M.L.; Reddy, K.R.; Liu, Z.P.; Jin, F. Effect of acid rain pH on leaching behavior of cement stabilized lead-contaminated soil. *J. Hazard. Mater.* **2014**, *271*, 131–140. [[CrossRef](#)]
28. Stanforth, R.; Yap, C.F.; Nayar, R. Effects of weathering on treatment of lead contaminated soils. *J. Environ. Eng.* **2005**, *131*, 38–48. [[CrossRef](#)]
29. Wu, Z.L.; Deng, Y.F.; Chen, Y.G.; Gao, Y.F.; Zha, F.S. Long-term desalination leaching effect on compression/swelling behaviour of Lianyungang marine soft clays. *Bull. Eng. Geol. Environ.* **2021**, *80*, 8099–8107. [[CrossRef](#)]
30. Zha, F.S.; Liu, J.J.; Xu, L.; Cui, K.R. Effect of cyclic drying and wetting on engineering properties of heavy metal contaminated soils solidified/stabilized with fly ash. *J. Cent. South. Univ.* **2013**, *20*, 1947–1952. [[CrossRef](#)]
31. Kalkan, E. Impact of wetting–drying cycles on swelling behavior of clayey soils modified by silica fume. *Appl. Clay Sci.* **2011**, *52*, 345–352. [[CrossRef](#)]
32. Zha, F.S.; Liu, S.Y.; Du, Y.J.; Cui, K.R. Behavior of expansive soils stabilized with fly ash. *Nat. Hazards* **2008**, *47*, 509–523. [[CrossRef](#)]
33. Hafsteinsdottir EG, White DA, Gore DB, Stark SC Products and stability of phosphate reactions with lead under freeze-thaw cycling in simple systems. *Environ. Pollut.* **2011**, *159*, 3496–3503. [[CrossRef](#)] [[PubMed](#)]
34. Wei, M.L.; Du, Y.J.; Reddy, K.R.; Wu, H.L. Effects of freeze-thaw on characteristics of new KMP binder stabilized Zn- and Pb-contaminated soils. *Environ. Sci. Pollut. Res. Int.* **2015**, *22*, 19473–19484. [[CrossRef](#)]
35. Zhou, Z.W.; Ma, W.; Zhang, S.J.; Mu, Y.H.; Li, G.Y. Effect of freeze-thaw cycles in mechanical behaviors of frozen loess. *Cold Reg. Sci. Technol.* **2018**, *146*, 9–18. [[CrossRef](#)]
36. Liu, J.J.; Zha, F.S.; Xu, L.; Kang, B.; Yang, C.B.; Feng, Q.; Zhang, W.; Zhang, J.W. Strength and microstructure characteristics of cement-soda residue solidified/stabilized zinc contaminated soil subjected to freezing–thawing cycles. *Cold Reg. Sci. Technol.* **2020**, *172*, 102992.
37. Zhao, R.F.; Zhang, S.N.; Gao, W.; He, J.; Wang, J.; Jin, D.; Nan, B. Factors effecting the freeze thaw process in soils and reduction in damage due to frosting with reinforcement: A review. *Bull. Eng. Geol. Environ.* **2019**, *78*, 5001–5010. [[CrossRef](#)]
38. Su, Y.Y.; Li, P.; Ren, Z.P.; Xiao, L.; Zhang, H. Freeze-thaw effects on erosion process in loess slope under simulated rainfall. *J. Arid. Land* **2021**, *12*, 937–949. [[CrossRef](#)]
39. Wei, H.B.; Jiao, Y.B.; Liu, H.B. Effect of freeze–thaw cycles on mechanical property of silty clay modified by fly ash and crumb rubber. *Cold Reg. Sci. Technol.* **2015**, *116*, 70–77. [[CrossRef](#)]
40. Wang, T.L.; Liu, Y.J.; Yan, H.; Xu, L. An experimental study on the mechanical properties of silty soils under repeated freeze–thaw cycles. *Cold Reg. Sci. Technol.* **2015**, *112*, 51–65. [[CrossRef](#)]
41. Yang, Z.; Li, X.; Li, D.; Wang, Y.; Liu, X. Effects of Long-Term Repeated Freeze-Thaw Cycles on the Engineering Properties of Compound Solidified/Stabilized Pb-Contaminated Soil: Deterioration Characteristics and Mechanisms. *Int. J. Environ. Res. Public Health* **2020**, *17*, 1798. [[CrossRef](#)] [[PubMed](#)]
42. Yang, Z.P.; Chang, J.Z.; Wang, Y.; Li, X.Y.; Li, S. Effects of Long-Term Freeze-Thaw Cycles on the Properties of Stabilized/Solidified Lead-Zinc-Cadmium Composite-Contaminated Soil. *Int. J. Environ. Res. Public Health* **2021**, *18*, 6114. [[CrossRef](#)] [[PubMed](#)]
43. Chen, X.D.; Lu, X.W.; Yang, G. Sources identification of heavy metals in urban topsoil from inside the Xi'an Second Ringroad, NW China using multivariate statistical methods. *Catena* **2012**, *98*, 73–78. [[CrossRef](#)]
44. Yao, Y.R.; Li, J.; He, C.; Hu, X.; Yin, L.; Zhang, Y.; Zhang, J.; Huang, H.Y.; Yang, S.G.; He, H.; et al. Distribution Characteristics and Relevance of Heavy Metals in Soils and Colloids Around a Mining Area in Nanjing, China. *Bull. Environ. Contam. Toxicol.* **2021**, *107*, 996–1003. [[CrossRef](#)] [[PubMed](#)]
45. Liu, H.B.; Liu, S.J.; He, X.S.; Dang, F.; Tang, Y.Y.; Xi, B.D. Effects of landfill refuse on the reductive dechlorination of pentachlorophenol and speciation transformation of heavy metals. *Sci. Total Environ.* **2021**, *760*, 144122. [[CrossRef](#)]
46. McLellan, B.C.; Williams, R.P.; Lay, J.; van Riessen, A.; Corder, G.D. Costs and carbon emissions for geopolymer pastes in comparison to ordinary portland cement. *J. Clean. Prod.* **2011**, *19*, 1080–1090. [[CrossRef](#)]
47. Cuisinier, O.; Le Borgne, T.; Deneele, D.; Masrouri, F. Quantification of the effects of nitrates, phosphates and chlorides on soil stabilization with lime and cement. *Eng. Geol.* **2011**, *117*, 229–235. [[CrossRef](#)]
48. Yang, Z.P.; Li, X.Y.; Wang, Y.; Chang, J.Z.; Liu, X.R. Trace element contamination in urban topsoil in China during 2000–2009 and 2010–2019: Pollution assessment and spatiotemporal analysis. *Sci. Total Environ.* **2020**, *758*, 143647. [[CrossRef](#)]
49. PeÁrez-Cid, B.; Lavilla, I.; Bendicho, C. Application of microwave extraction for partitioning of heavy metals in sewage sludge. *Anal. Chim. Acta* **1999**, *378*, 201–210. [[CrossRef](#)]
50. Liu, D.D.; Miao, D.R.; Liu, F. Evaluation of the As, Cu and Pb Immobilizing Efficiency by Tessier, TCLP and SBET Method. *Adv. Mater. Res.* **2014**, *878*, 520–521. [[CrossRef](#)]
51. Linker, R.; Shmulevich, I.; Kenny, A.; Shaviv, A. Soil identification and chemometrics for direct determination of nitrate in soils using FTIR-ATR mid-infrared spectroscopy. *Chemosphere* **2005**, *61*, 652–658. [[CrossRef](#)] [[PubMed](#)]

52. Shi, T.; Yang, Z.P.; Zheng, L.W. FTIR spectra for early age hydration of cement-based composites incorporated with CNTs. *Acta Mater. Compos. Sin.* **2017**, *34*, 653–660.
53. Yan, K.Z.; Guo, Y.X.; Li, N.J.; Cheng, F.Q. Effect and Mechanism Analysis of Calcium Oxide Additive on the Sodium Carbonate Activation of Fly Ash. *Bull. Chin. Ceram. Soc.* **2018**, *37*, 1003–1009.
54. Correia, A.A.S.; Matos, M.P.S.R.; Gomes, A.R.; Rasteiro, M.G. Immobilization of Heavy Metals in Contaminated Soils—Performance Assessment in Conditions Similar to a Real Scenario. *Appl. Sci.* **2020**, *10*, 7950. [[CrossRef](#)]
55. Guo, B.; Liu, B.; Yang, J.; Zhang, S.G. The mechanisms of heavy metal immobilization by cementitious material treatments and thermal treatments: A review. *J. Environ. Manag.* **2017**, *193*, 410–422. [[CrossRef](#)] [[PubMed](#)]
56. Zha, F.S.; Liu, C.M.; Kang, B.; Yang, X.H.; Zhou, Y.; Yang, C.B. Acid rain leaching behavior of Zn-contaminated soils solidified/stabilized using cement-soda residue. *Chemosphere* **2021**, *281*, 130916. [[CrossRef](#)]
57. Fei, Y.; Yan, X.L.; Zhong, L.R.; Li, F.S.; Du, Y.J.; Li, C.P.; Lv, H.Y.; Li, Y.H. On-Site Solidification/Stabilization of Cd, Zn, and Pb Co-Contaminated Soil Using Cement: Field Trial at Dongdagou Ditch, Northwest China. *Environ. Eng. Sci.* **2018**, *35*, 1329–1339. [[CrossRef](#)]
58. Zhang, W.L.; Zhao, L.Y.; Yuan, Z.J.; Li, D.Q.; Morrison, L. Assessment of the long-term leaching characteristics of cement-slag stabilized/solidified contaminated sediment. *Chemosphere* **2021**, *267*, 128926. [[CrossRef](#)]
59. Yoon, D.H.; Choi, W.S.; Hong, Y.K.; Lee, Y.B.; Kim, S.C. Effect of chemical amendments on reduction of bioavailable heavy metals and ecotoxicity in soil. *Appl. Biol. Chem.* **2019**, *62*, 1–7. [[CrossRef](#)]
60. Bai, B.; Nie, Q.K.; Zhang, Y.K.; Wang, X.L.; Hu, W. Cotransport of heavy metals and SiO₂ particles at different temperatures by seepage. *J. Hydrol.* **2021**, *597*, 125771. [[CrossRef](#)]
61. Ouhadi, V.R.; Yong, R.N.; Deiranlou, M. Enhancement of cement-based solidification/stabilization of a lead-contaminated smectite clay. *J. Hazard. Mater.* **2021**, *403*, 123969. [[CrossRef](#)] [[PubMed](#)]
62. Velichenko, A.B.; Portillo, J.; Sarret, M.; Muller, C. Zinc dissolution in ammonium chloride electrolytes. *J. Appl. Electrochem.* **1999**, *29*, 1119–1123. [[CrossRef](#)]
63. Mitani, T.; Ogawa, M. Cadmium leaching by acid rain from cadmium-enriched activated sludge applied in soil. *J. Environ. Health* **1998**, *33*, 1569–1581. [[CrossRef](#)]